Title

Lithium dendrite growth mechanisms in polymer electrolytes and prevention strategies

Journal

Physical Chemistry Chemical Physics, 19(31)

ISSN

0956-5000

Authors

Barai, Pallab

Higa, Kenneth

Srinivasan, Venkat

Publication Date

2017-08-09

DOI

10.1039/c7cp03304d

Lithium Dendrite Growth Mechanisms in Polymer Electrolytes and Prevention Strategies

Pallab Barai[1], Kenneth Higa[2] and Venkat Srinivasan[1z]

[1]Argonne National Laboratory, Lemont, Illinois 60439 USA

[2]Lawrence Berkeley National Laboratory, Berkeley, California 94720 USA

Revised version for submission in

Physical Chemistry Chemical Physics

June 2017

---

[z]Corresponding author: Venkat Srinivasan (email: vsrinivasan@anl.gov)

Abstract

Future lithium-ion batteries must use lithium metal anodes to fulfill the demands of high energy density applications with the potential to enable affordable electric cars with 350-mile range. However, dendrite growth during charging prevents the commercialization of this technology. It has been demonstrated that the presence of a compressive mechanical stress field around a dendritic protrusion prevents growth. Several techniques based on this concept, such as protective layers, externally applied pressure and solid electrolytes have been investigated by other researchers. Because of the low coulombic efficiencies associated with the stiff protective layers and high-pressure conditions, implementation of these techniques in commercial cells is complicated. Polymer-based solid electrolytes demonstrate better efficiency and capacity retention capabilities. However, dendrite growth is still possible in polymer electrolytes at higher current densities. The simulations described in this article provide guidance on the conditions under which dendrite growth is possible in polymer cells and targets for material properties needed for dendrite prevention. Increasing the elastic modulus of the electrolyte prevents the growth of dendritic protrusions in two ways: i) Higher compressive mechanical stress leads to reduced exchange current density at the protrusion peak compared to the valley, and ii) Plastic deformation of lithium metal results in reduction of the height of the dendritic protrusion. A phase map is constructed, showing the range of operation (applied current) and design (electrolyte elastic modulus) parameters that corresponds to stable lithium deposition. It is found that increasing the yield strength of the polymer electrolyte plays a significant role in preventing dendrite growth in lithium metal anodes, providing a new avenue for further exploration.

Keywords: *lithium metal anode, dendrite growth, current distribution, elastic-plastic deformation, yield strength*

Graphical Abstract

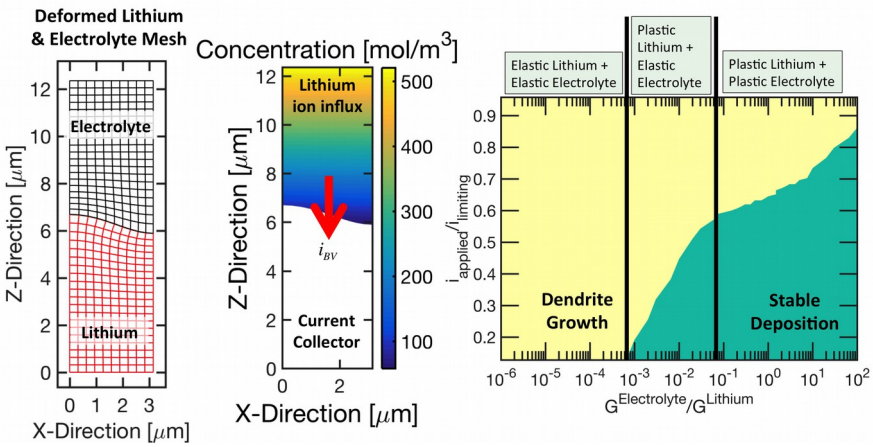

Demonstration of the computational domain, the concentration profile within electrolyte and a phase map between applied current and electrolyte modulus showing the domains where suppression of dendritic protrusions is possible.

Introduction

Lithium metal anodes, with low reduction potential (-3.04V) and high specific capacity (3870mAh/g), are essential for the development of next-generation lithium-ion batteries (LIBs) with improved energy and power density[1]. However, uncontrollable dendrite growth during the recharge process inhibits the application of lithium metal anodes in commercially-available rechargeable LIBs[2]. Suppression of dendrite growth by the application of mechanical stress is considered to be an effective technique for cycling lithium metal anodes without the formation of dendrites[3-6]. Solid polymer electrolytes (SPEs)[7, 8], robust separators[3], protective layers[9, 10] and stiff solid electrolyte interface (SEI) layers[2, 4, 6] have been investigated to obtain dendrite-free lithium metal anodes over multiple charge-discharge cycles. Unfortunately, these techniques either have limited success in preventing the growth of dendrites, or introduce other challenges (such as, increased interfacial resistance, either due to insufficient contact area or because of slow ionic and/or electronic transport through the interfacial layer), which render them unsuitable for application in commercial products. For example, due to the low ionic conductivity of SPEs at room temperature, it is necessary to operate the polymer electrolyte batteries at elevated temperatures[11]. The elastic stiffness of the polymers decreases significantly at higher temperature[12], and needle-like dendrites can easily grow resulting in a short circuit[13, 14]. Cycling with stiff SEI layers on top of lithium metal results in low coulombic efficiency[6], and rupture of the SEI leads to dendrite growth[15, 16]. Deterioration of the interfacial resistance between lithium metal and robust separators render them less useful over multiple cycles[17, 18]. Among these different techniques of preventing dendrite growth, SPEs are the most promising candidates for commercial implementation[19] because block-polymers can be synthesized with a combination of superior properties[20]. How solid

electrolytes prevent the growth of dendrites during operation at high current densities must be properly understood for the successful design of low-cost dendrite-free solid polymer electrolytes[21-23].

Transport limitations are usually attributed as the major reasons behind the formation of dendrites on lithium metal anodes[24, 25], which is generally observed under high current density and low-temperature operation[13, 24, 26]. It has been argued that in liquid electrolytes before the onset of electrolyte diffusion limitation, characterized as operation at current densities below the limiting current, lithium deposition happens at the base of the dendritic protrusion[3], leading to the growth of mossy lithium. However, at the onset of electrolyte diffusion limitation, observed at current densities higher than the limiting current, lithium ions from the electrolyte instead deposit at the tips of the dendritic protrusions[3]. This leads to the growth of dendritic structures capable of internally shorting the cell. However, there is evidence of dendrite growth and subsequent short circuit at current densities much lower than the limiting current[27, 28]. This can be attributed to either the onset of diffusion limitation even at currents lower than the limiting value, or the localization of current at certain points due to microstructural heterogeneity.

It has been argued that, if the diameters of the propagating dendrites are smaller than the size of the pores present within the polymer electrolyte/separator, the dendrites may pierce through the polymer layer [3, 7]. The size of a dendritic protrusion inversely depends on the overpotential and the applied current density[29]. At higher applied current densities, large overpotentials are observed, which leads to the formation of lithium dendrite nuclei with relatively small diameters. Hence, lithium deposition at high rates has the potential to form needle-like dendrites that can easily penetrate through the pores of the separator, and

subsequently short-circuit the cell[3, 7]. However, it has also been argued that the pores within the polymeric separator are in the range of tens of nanometers[30]. Whereas, the needle like dendrites that penetrate through the separator has diameter in the range of microns[31]. Hence, the dendrites that short circuit the cell grow by penetrating the polymer, rather than by going through the pores[8, 11].

Several theoretical studies have been performed to capture the growth of dendrites in related systems. Barton and Bockris conducted the first quantitative analyses of dendrite growth on metal during electrochemical deposition[32]. They considered the overpotentials associated with activation, diffusion and surface curvature effects, and concluded that the maximum velocity of dendrite growth is a function of the applied overpotential. Later, Diggle *et al.* analyzed the current distribution around a dendritic protrusion using Butler-Volmer reaction kinetics[33]. They concluded that the overpotential associated with the surface curvature prevents infinite thinning of the propagating dendrite tip. Chazalviel concluded that dendrite growth is always associated with diffusion limitations, ion depletion and generation of a space charge near the electrode[34]. This indicated that initiation and propagation of dendrites is only possible at current densities greater than the limiting current. On the contrary, Monroe and Newman demonstrated that if a lithium nucleus exists, it will propagate[35] with a rate dependent on the applied current density, local radius of curvature and local concentration of lithium ions within the electrolyte. These conclusions were supported by Akolkar, who modeled the dendrite growth process using transient diffusion of lithium coupled with activation, concentration, and overpotentials induced by surface curvature[36]. At lower operating temperatures, reduced diffusion coefficient and increased cathodic transfer coefficient values resulted in enhanced dendrite growth[37]. Solving for potential and concentration distributions

within the electrolyte, Cogswell explored the role of competition between reaction rate and diffusion rate in dendrite growth[25]. High diffusivity of lithium ions within the electrolyte and low exchange current density of the lithium reduction reaction led to stable deposition. Others have used phase-field techniques to investigate the impact of electrode surface morphology on dendrite growth [38-40].

It has been experimentally demonstrated that prevention of dendritic protrusion is possible by the means of mechanical stress[5, 41]. However, proper understanding of how the stress field suppresses dendrite growth is significantly lacking. Monroe and Newman developed the background theoretical work necessary to understand the impact of mechanical stress on reaction current[42]. Under the assumption of a pre-stressed lithium surface and elastic deformation, they concluded that the shear modulus of the solid polymer electrolyte/separator needs to be approximately two times larger than that of lithium metal for successful suppression of dendrite growth[23]. The assumption of pre-stressed lithium was relaxed by Barai *et al.*, who then demonstrated that dendrite growth is never observed during relatively low current density operations[21]. It has also been argued by Ferrese and Newman that plastic deformation of lithium metal occurs at the lithium-separator interface during deposition[22]. There is experimental evidence of uniform deposition due to probable plastic deformation of lithium metal under externally applied pressure[43, 44] or with the use of stiff separators[45, 46]. However, along with the plastic deformation of lithium[47], polymer-based separators/electrolytes also demonstrate plasticity[12]. The elastic-plastic deformation of both lithium and polymer affect the overall dendrite growth process.

According to the pioneering work by Monroe and Newman (*JES*, 2005) it is possible to prevent the growth of dendritic protrusions by using an electrolyte with shear modulus two

times larger than metallic lithium [23]. However, recently it has been observed that even PEO type polymer based electrolytes can impact the growth of dendritic protrusions [8]. Since, the elastic modulus of PEO is approximately two to three orders of magnitude smaller than that of lithium, this polymeric electrolyte is unable to completely prevent the growth of dendrites. But its impact on the overall dendrite growth is evident from the increase in diameter and parabolic shape of the protrusion, as compared to needle like dendrites observed in liquid electrolytes. Analyzing the propensity of growth of a dendritic protrusion, taking into account the possibility of plastic deformation within both metallic lithium as well as the polymer electrolyte, has not been investigated earlier. In the present article, a computational technique has been developed for the first time that can correctly capture the evolution of stress within both lithium and electrolyte by appropriately taking into account the elastic-plastic deformation. The combined impacts of mechanical stress distribution and transport limitations on the propagation of dendritic protrusions will be investigated for the first time. Using the model developed here, a critical current density (as a ratio with respect to the limiting current) will be determined, below which dendrite growth should not occur for PEO-based electrolytes[7]. A phase map between the applied current density and the polymer shear modulus is constructed, depicting the regime where stable deposition of lithium is expected. Some modifications to the yield strength of present-day polymer electrolytes will be suggested that can potentially suppress the growth of dendritic protrusions.

Methodology

The present work examines the propensity for growth of a dendritic protrusion on a lithium metal electrode. Operation at low as well as high current density has been considered[13,

24]. Elastic-plastic deformations of both lithium metal and PEO-based polymer electrolyte have been taken into account[48, 49]. To capture the correct mechanical deformation of the lithium metal anode, dendritic protrusion and polymer electrolyte, the momentum balance (equilibrium) equation has been solved throughout the system[50]. For estimation of the current distribution, the primary current (due to potential gradient), secondary current (due to electrode kinetics) and tertiary current (due to concentration gradient) have been calculated[51]. This requires solving the charge and mass conservation equations coupled with the nonlinear Butler-Volmer electrode kinetics relation[52]. Detailed descriptions of these governing differential equations, along with boundary conditions, have been provided in the supplementary section.

The present analysis considers a spatial domain with lithium and electrolyte regions. Figures 1(a) and 1(b) show schematic representations of mechanical deformation and lithium transport. The dendritic protrusion has been generated by applying a sinusoidal vertical interfacial displacement, which has the form, $u_z = A\cos(\omega x)$ [23]. The protrusion height is defined as the distance between the peak and the valley $(H = 2A)$, as noted in Figure 1(a). Dendritic protrusion heights have been reported to range from nanometers to microns[31, 53, 54]. Using scanning and/or transmission electron microscopy techniques, dendritic protrusions in liquid electrolytes were observed to range in height between 500nm – 1000nm [53, 55]. The time-of-flight-secondary-ion-mass-spectroscopy (ToF-SIMS) images revealed the height of lithium nucleus to be around 200nm in a system using EC/DMC-based solvent and $LiPF_6$

salt[31]. In the present simulations, the amplitude of the dendritic protrusion has been taken to be $A = 400nm$, corresponding to a protrusion height of $H = 800nm$. To remain consistent with the initial aspect ratio introduced by Monroe and Newman in their *JES* 2005 article[23], the frequency of the interfacial displacement has been considered to be $\omega = 10^6 m^{-1}$.

Finally, the concentration and potential within the lithium metal and polymer electrolyte have been solved as indicated in Figure 1(b). The reaction current at the lithium-electrolyte interface was estimated from the modified Butler-Volmer equation[42]. The effect of mechanical stress was incorporated within the exchange current density term[23]. An influx of lithium ions was imposed on the top electrolyte boundary. The bottom boundary of the lithium region served as a current collector. Symmetric boundary conditions of zero current and zero ionic flux were applied at the left and right boundaries. For a detailed description of how the computation was conducted, please refer to the supplementary section.

Electrochemical equations: Transport of lithium ions within the electrolyte phase may happen through diffusion and migration processes. During the charging process, lithium gets reduced at the metal anode as [23]:

$$Li^+ + e^- \rightarrow Li\downarrow \quad (1)$$

Since lithium gets plated on top of the electrode, no lithium transport equation needs to be solved within the lithium metal anode phase. However, charge transport within the electrolyte and the metallic anode phase must be determined[51, 52]. Also, local charge neutrality must be satisfied everywhere to ensure no accumulation of electric charge anywhere within the electrolyte or

metallic lithium. This is accomplished by setting the time-dependent accumulation terms to zero within the charge transport equations.

Current associated with the reduction of lithium ions $\left(i_{BV}\right)$ at the metal/electrolyte interface can be estimated using the Butler-Volmer equation. The activation over-potential required for this electrochemical reaction to occur is denoted by η. The Butler-Volmer equation is represented as[23, 35]:

$$i_{BV} = Fk_a^{\alpha_c}\left(k_c c_e\right)^{\alpha_a} \exp\left(\frac{\alpha_a \Delta\mu_{e^-}}{RT}\right)\left[\exp\left(\frac{\alpha_a F\eta}{RT}\right) - \exp\left(-\frac{\alpha_c F\eta}{RT}\right)\right]. \quad (2)$$

Here, k_a and k_c are the anodic and cathodic reaction rate constants, and α_a and α_c are the anodic and cathodic transfer coefficients, respectively. Also, $\Delta\mu_{e^-}$ indicates the electrochemical potential change induced by mechanical stresses and surface curvature effects, which will be discussed in detail later in this article (see Eq. (3))[23]. Moreover, F denotes Faraday's constant, R denotes the universal gas constant and T signifies the local temperature on the Kelvin scale. For the reduction of lithium ions at the lithium metal anode, the anodic and cathodic rate

constants are assumed to be equal $\left(k_a = k_c\right)$ [52]. Also, the anodic and cathodic transfer coefficients have been assumed to be equal for reduction of lithium metal by several other researchers[22, 35, 40], so that $\alpha_a = \alpha_c = 1/2$ [52]. The magnitude of over-potential at the lithium-electrolyte interface is estimated as $\eta = \phi_s - \phi_e - U_{Li}$, which takes a negative value during the reduction process. Here, ϕ_s and ϕ_e indicate the solid phase potential and electrolyte phase potential, respectively. The open circuit potential for lithium metal has been denoted by U_{Li}, which is taken to be zero[42].

For modeling the ion and charge transport, zero interfacial resistance between lithium metal and polymer electrolyte has been assumed[35]. Also, side reactions on the lithium metal surface have been neglected[38]. However in a realistic scenario, side reactions on the lithium metal surface would form a solid electrolyte interface (SEI) layer, which along with the inherent roughness of metallic lithium would lead to an imperfect interface with significant interfacial resistance[2]. These imperfections can give rise to higher activation polarization at the lithium/electrolyte interface.

Mechanics equations: Since the stress values around the dendritic protrusion appear within the modified Butler-Volmer relation (see Eq. (2)), mechanical deformation of lithium metal and polymer electrolyte must be determined appropriately. Since mechanical equilibration occurs at the speed of sound, it is much faster than the chemical reactions that occur at the lithium-electrolyte interface[56]. Hence the quasi-static equilibrium equation, derived from the momentum balance relation, should be solved to capture the stress field[22, 23, 42, 50]. Also, under the application of sufficiently large tensile or compressive loads, all bulk materials deform in an elastic-plastic fashion[57]. Lithium metal and polymer electrolytes are no exception to that. Hence, to determine the appropriate stress field around a dendritic protrusion, the exact elastic-plastic nonlinear stress-strain constitutive relations must be taken into consideration[12, 47]. To describe the elastic portion, Young's modulus (and) and Poisson's ratio (and) are sufficient. These are readily available in the literature for both lithium metal as well as PEO-based polymers[12, 49]. Characterizing the plastic deformation of lithium and the polymer electrolyte is more challenging. In the present context, a nonlinear hardening law has been used for the metal and polymer phases as shown in the Supplementary section (see Eq. (S20)).

E_{Li} E_{PEO} ν_{Li} ν_{PEO}

Mechanical stress induced electrochemical potential: The effect of the mechanical stress field on the dendrite growth process has been modeled by modifying the Butler-Volmer equation. A new electrochemical potential term has been defined and incorporated into the reaction

$\left(\Delta\mu_{e^-}\right)$

current density $\left(i_{BV}\right)$ expression (see Eq. (2)). Contributions form hydrostatic stress $\left(\sigma_{kk}=\sigma_{11}+\sigma_{22}+\sigma_{33}\right)$, deviatoric stress $\left(s_{ij}\right)$ and local surface curvature $\left(\kappa\right)$ are present within the expression of the electrochemical potential $\left(\Delta\mu_{e^-}\right)$, which varies along the x-direction[23, 42]:

$$\begin{aligned}\Delta\mu_{e^-}\left(x\right)=&-\frac{1}{2}\left(\bar{V}_{Li}+\left(1-t_{LI^+}\right)\bar{V}_{Elec}\right)\cdot\\&\cdot\left\{-\gamma\kappa+\vec{n}\bullet\left[\vec{n}\bullet\left(\Delta\underset{\approx}{\tau}^{Lithium}-\Delta\underset{\approx}{\tau}^{Electrolyte}\right)\right]\right\}+\\&+\frac{1}{2}\left(\bar{V}_{Li}-\left(1-t_{LI^+}\right)\bar{V}_{Elec}\right)\cdot\left(\Delta p^{Lithium}+\Delta p^{Electrolyte}\right)\end{aligned} \quad . \quad (3)$$

Here, $\bar{V}_{Li}$ and $\bar{V}_{Elec}$ represent the partial molar volume of lithium and electrolyte salt, respectively, γ is the surface energy, and $\vec{n}$ represents the normal vector at the lithium-electrolyte interface. The pressure term is calculated as $\Delta p^{Lithium}=-\sigma_{kk}^{Lithium}/3$ and

$\Delta p^{Electrolyte} = -\sigma_{kk}^{Electrolyte} \big/ 3$, and the deviatoric stress terms are evaluated as $\Delta \tau_{ij}^{Lithium} = -s_{ij}^{Lithium}$ and $\Delta \tau_{ij}^{Electrolyte} = -s_{ij}^{Electrolyte}$. Repeated indices indicate implicit summation throughout this entire article wherever indicial notations have been used. In this 2D computational domain, the local curvature κ has been calculated in a piece-wise fashion[58].

In our computational procedure, the decrease in height of the dendritic protrusion due to compression from the electrolyte is evaluated first, satisfying mechanical equilibrium. The resulting deformed configuration of the lithium-electrolyte system is then adopted as the domain for solving the transport and potential equations. All the results reported in the subsequent sections have been obtained by solving the deformation-transport problem in this two-step procedure.

Results and Discussion

To analyze the propensity of growth of a dendritic protrusion, the difference in reaction current density at the peak of the protrusion $\left(i_{peak}\right)$ can be compared with that at the valley $\left(i_{valley}\right)$ [21, 23]. If the current at the peak is greater than the current at the valley $\left(i_{peak} > i_{valley}\right)$, the

dendrite should grow because more lithium deposition occurs at the protrusion peak as compared to the valley. Otherwise, when the current at the protrusion peak is smaller than or equal to the current at the valley $\left(i_{peak} \leq i_{valley}\right)$, stable deposition of lithium is expected to occur without the development of dendrites. The local reaction current is obtained from the Butler-Volmer relation (see Eq. (2))[23]. Its magnitude depends on the mechanical stress field (through the term $\Delta\mu_{e^-}$), potential distribution (through η) and concentration of lithium ions within the electrolyte (in the form of c_e) around the dendritic protrusion. In the present research, we will determine design conditions (in terms of material properties of the polymer electrolyte) and operational conditions (in terms of applied current density), which lead to higher reaction current at the valleys as compared to the protrusion peaks; thereby preventing dendrite growth.

However, to construct such a correlational phase map, it is necessary to appropriately model the elastic-plastic stress-strain relations observed in lithium metal and polymer electrolytes. The nonlinear stress-strain relations have already been described. To determine the correct elastic (Young's modulus and Poisson's ratio) and plastic (yield strength, strain hardening modulus and hardening exponent) parameters for the bulk lithium metal and PEO-based polymer electrolyte, comparison with experimental results is required.

Elastic-plastic stress-strain relations: There is ample evidence that under sufficiently large magnitudes of stress, both lithium metal as well as the polymer electrolyte phase deform in an elastic-plastic fashion[12, 47-49]. The three material parameters necessary for appropriately modeling the plastic response are yield strength (and), hardening modulus (and) and hardening exponent (and)[57]. Figures 2(a) and 2(b) show fits to published experimental results used to obtain elastic and plastic parameters for both metallic lithium and polymer electrolytes. To obtain the experimental elastic-plastic stress-strain curve for bulk lithium, Schultz applied uniaxial tensile load on a piece of lithium metal[47]. The experimentally observed elastic-plastic stress-strain curve for PEO-based polymer has been adopted from measurements published by Geng *et al*., who used a dynamic mechanical analyzer at room temperature conditions[12]. Elastic-plastic properties of PEO-based polymers have been observed to change with its molecular weight[59]. The molecular weight of the polymer used in this experiment was reported as 30,000g/mol[12].

$\sigma_{0,Li}$ $\sigma_{0,PEO}$ H_{Li} H_{PEO} m_{Li} m_{PEO}

The elastic-plastic parameters of lithium metal and polymer electrolyte, extracted from comparison with the experimental results, will be used for simulating the evolution of the stress field around the dendritic protrusion. The Young's modulus of lithium metal is almost two orders of magnitude greater than the PEO-based polymer electrolyte[12, 47]. On the contrary, the yield

strength of lithium metal is smaller than the yield strength of polymer electrolyte $\left(\sigma_{0,Li} < \sigma_{0,PEO}\right)$.

This variation in Young's modulus and yield strength significantly impacts the overall dendrite growth process. These elastic-plastic properties of lithium have been used in all subsequent simulations. For PEO-based polymers, the elastic-plastic properties determined here will be adopted. For other polymers with elastic modulus values different from PEO, different elastic properties (such as shear modulus and Poisson's ratio) will be used. However, the plastic properties (such as, yield strength, hardening modulus and hardening exponent) of PEO-based polymers have been used everywhere for the lack of sufficient data.

Effect of applied current density: It is well-known that lithium dendrite growth occurs during electrochemical deposition of metallic lithium on top of lithium foil (or other metallic electrodes). Without any applied current, no dendrites should grow[60]. Although applied current density can drive dendrite growth, externally applied mechanical stress can prevent the growth of dendrites under certain circumstances[21, 23]. To understand the impact of applied stress on the reaction current around the dendritic protrusion, one must solve for the variation of concentration and potential within the lithium metal and electrolyte[35, 36].

The potential and concentration contours obtained at steady state during operation at 75% of the limiting current density are shown in Figures 3(a) and 3(b), respectively. Significant differences in both potential and concentration between the peak and the valley of the dendritic protrusion are evident in the figures. Due to the very high conductivity of lithium metal, the solid phase potential remains very close to zero within metallic lithium[38]. Hence, the solid phase potential is not shown in the potential contour plot (Figure 3(a)). Deposition of lithium happens at the lithium-electrolyte interface, and no transport of lithium ions occurs within the metallic

phase. Hence, Figure 3(b) does not show a concentration profile within the lithium metal. An initial protrusion height of 800nm and very low polymer electrolyte shear modulus $\left(G^{Electrolyte} = 10^{-5} G^{Lithium}\right)$ was used to generate the potential and concentration contours. The extremely low elastic modulus of the polymer electrolyte does not produce any significant mechanical suppression of the dendritic protrusion height, which enhances the difference in concentration and potential profiles between the peak and the valley.

The 800nm high dendritic protrusion is consistent with several reports of protrusion height ranging from 500nm to 1000nm [31, 53, 55]. From Figures 3(a) and 3(b) it is obvious that both the potential and the concentration at the valley are smaller in magnitude than that at the peak. This difference in potential and lithium-ion concentration between the peak and the valley of the dendritic protrusion leads to a difference in reaction current, usually calculated using the Butler-Volmer relation, in two ways:

i) Variation in salt concentration impacts the local conductivity, which results in formation of a potential gradient between the peak and valley of the dendritic protrusion. Variation in electrolyte potential due to the difference in height of the protrusion peak and valley also exists and is particularly evident under low current density operation.
ii) The reference exchange current density usually depends on the local electrolyte concentration[61]. Variation in lithium-ion concentration between the peak and valley also leads to a difference in the magnitude of reference exchange current density at those two points.

If the current at the peak $\left(i_{peak}\right)$ is greater than the current at the valley $\left(i_{valley}\right)$, then the dendrite will grow. Otherwise, stable deposition of lithium is expected to occur. For PEO-based polymer electrolytes, due to mechanical suppression of the dendritic protrusion, the dendrite height is reduced to approximately 580nm. This leads to a quantitatively different, but qualitatively similar, concentration and potential profile as compared to the 800nm high dendritic protrusion.

Next, we will determine the applied current density range over which a dendritic protrusion in a lithium-polymer system can grow to form a needle-like dendrite. Concentration and potential contours at three different current densities of 1%, 50% and 90% of the limiting current are shown in Figures S3(a), S3(b) and S3(c). Larger gradients in the concentration and the potential field are seen during operation at higher current densities.

To determine the propensity of growth of a dendritic protrusion, the reaction current densities at the peak and the valley have been estimated from Eq. (2). The electrochemical potential term $\left(\Delta\mu_{e^-}\right)$ has been calculated using Eq. (3). The magnitudes of deviatoric and hydrostatic stresses have been predicted by solving the equilibrium equation. Elastic-plastic deformation within both lithium metal and PEO-based polymer electrolyte phase has been assumed, which leads to changes in the interfacial geometry. The potential and concentration equations have been solved on top of this modified geometry. The reaction currents have been estimated at the peak and the valley according to the Butler-Volmer equation for different values of the applied current. Figure 4 shows the ratio of current between the peak and the valley

with respect to the applied current as a fraction of limiting current $\left(i_{peak}/i_{valley}\right)$. If $\left(i_{applied}/i_{\text{limiting}}\right)$

the current ratio between the peak and the valley is greater than unity $\left(\left(i_{peak}/i_{valley}\right)>1\right)$,

dendrites will grow. Otherwise, stable deposition of lithium is expected to occur under the

condition $\left(\left(i_{peak}/i_{valley}\right)<1\right)$. The blue horizontal line in Figure 4 demarcates this limit. From the

figure, it is clear that for a lithium-PEO system, dendrite growth should not occur for applied current densities smaller than 42% of the limiting current density (no dendrite growth at $i_{applied}<0.42\times i_{limiting}$). The results also indicate that for PEO-based electrolytes, growth of

dendritic protrusions are possible at applied current densities greater than 42% of the limiting

current (dendrite growth at $i_{applied}>0.42\times i_{limiting}$). Hence, it can be concluded that in PEO based

polymer electrolytes, lithium dendritic protrusions can propagate at current densities much smaller than the limiting current, which correlates very well with certain experimental observations[27]. No current density above the limiting current has been analyzed here.

To validate the applicability of these results, the computational predictions have been qualitatively compared with some experimental observations. Brissot *et al.* conducted direct *in*

situ observation of dendrite growth during electrochemical deposition in a lithium/PEO system[7]. They estimated a limiting current density of $1.8A/m^2$ in a 1.2mm thick polymer electrolyte layer[7]. At a current density of $0.3A/m^2$, approximately 16% of the limiting current, it was reported that no dendritic growth occurred[7]. This data point representing no dendrite growth is shown by the blue plus (+) symbol in Figure 4. Growth of dendrites has been observed experimentally at applied current densities of 55% and 100% of the limiting current[7]. The red symbols within Figure 4 denote these two data points. The experimental data shows the same trend as the prediction with a cut-off between the growth to stability regime being around 0.4 $i_{limiting}$. While the predictions are consistent, a more detailed comparison is not possible because of the differences in the simulation domain versus the experimental thickness of the separator.

Effect of electrolyte stiffness: Elastic stiffness of the electrolyte phase affects the deposition of lithium on top of the metal substrate[3, 41, 45]. During lithium deposition at the lithium-electrolyte interface, the assumption of elastic deformation of lithium metal and polymer electrolyte is not realistic[12, 47]. The stress that evolves around the dendritic protrusion can exceed the elastic limit of both lithium and PEO-based polymer material. For very soft electrolytes ($G^{Electrolyte} < 10^{-4}\ G^{Lithium}$), the effective stresses that evolve within the lithium and electrolyte phases are significantly smaller than the corresponding yield limits (also demonstrated in Figure S4(a)). Hence, only elastic deformation is expected to occur. However, for slightly stiff PEO-based electrolytes ($G^{Electrolyte} \sim 10^{-2}\ G^{Lithium}$), the effective stress within the lithium metal exceeds its yield limit (see Figure S4(b)). Though the effective stress in the PEO electrolyte remains below the yield limit of the material, it can easily exceed the yield strength for stiffer materials. Hence, nonlinear elastic-plastic deformation of both lithium and electrolyte

must be incorporated while investigating the impact of electrolyte shear modulus on the overall growth of dendrites.

During operation at low current densities, the mechanical stress field at the protrusion peak and the valley dictates the corresponding ratio of current densities to a significant extent[21, 23]. To appropriately predict the magnitude of the stress field, proper nonlinear elastic-plastic deformation of the lithium metal and PEO-based polymer electrolyte has been considered. However, at larger current densities, potential and concentration gradient also plays a significant role in estimating the reaction current density at the peak and the valley of the dendritic protrusion[17, 35, 36]. Figure 5 shows the ratio of current density at the protrusion peak over that at the valley $\left(i_{peak}/i_{valley}\right)$ with respect to the normalized shear modulus of electrolyte $\left(G^{Electrolyte}/G^{Lithium}\right)$. The applied current density $\left(i_{applied}\right)$ is approximately 75% of the limiting current $\left(i_{limiting}\right)$. During operation at higher current densities, the combined effect of concentration/potential gradient and elastic-plastic deformation of lithium leads to the conclusion that the electrolyte shear modulus has to be approximately 20 times greater than lithium for stable deposition. There are two competing factors that determine the growth of dendrites:

i) The compressive mechanical stress field around the protrusion prevents the growth of dendrites.

ii) The potential and concentration difference between the peak and the valley enhances deposition of lithium at the protrusion peak and subsequent growth of dendrites.

The expression of reaction current is given by the Butler-Volmer equation provided in Eq. (2). The entire expression can be divided into two parts:

i) The mechanical stress factor, which will be called the "interfacial-stress factor" of the reaction current density is given by the expression: $\exp\left(\left(\alpha_a \times \Delta\mu_{e^-}\right)/RT\right)$

ii) The concentration/overpotential factor of the reaction current density, given by:

$$Fk_a^{\alpha_c}\left(k_c c_e\right)^{\alpha_a}\left[\exp\left(\frac{\alpha_a F\eta}{RT}\right)-\exp\left(-\frac{\alpha_c F\eta}{RT}\right)\right]$$

The ratio of the interfacial-stress factors at the protrusion peak and valley is shown by the blue triangles in Figure 5, while the ratio of the concentration/overpotential factors at the peak and valley of the dendritic protrusion is shown by the red squares. With increasing magnitude of the electrolyte shear modulus, both the interfacial-stress factor and concentration/overpotential factor can act to suppress the growth of dendrites. As the shear modulus of the electrolyte phase increases, the enhanced mechanical compressive stress field prevents the deposition of lithium at the protrusion peak, which eventually decreases the current ratio[21, 23, 42]. For high shear modulus electrolytes, plastic deformation of lithium metal significantly decreases the height of the dendritic protrusion. The variation in concentration/potential gradient-induced current ratio

with increasing electrolyte modulus can be attributed to this change in geometry of the lithium-polymer interface[43].

Experimental evidence indicates that with ionic liquid-based electrolytes, dendrite-free cycling is possible even with a shear modulus in the range of tens of kilopascals (~$10^4 N/m^2$)[62]. On the other hand, at current densities greater than the limiting current, dendrite growth has been observed even with ceramic separators[3], which has a shear modulus around 100 times larger than that of metallic lithium[63]. However, the mechanism behind dendrite growth within ceramics has been attributed to the presence of grain/grain-boundary microstructure and localization of current at the grain-boundary region. Hence, both applied current density and electrolyte shear modulus are important in estimating the propensity of dendrite growth. To understand the competition between mechanical stress-induced suppression and concentration/potential gradient-induced enhancement of dendritic protrusions, it is worthwhile to develop a phase map showing the effects of applied current density (normalized by the limiting current) and electrolyte shear modulus (normalized by the lithium shear modulus) on dendrite growth. Figure 6 provides such a phase map, where the light green portion indicates stable deposition (mathematically represented by $\left(i_{peak}/i_{valley}\right)<1$), and the yellow region denotes growth of dendrites (mathematically represented by $\left(i_{peak}/i_{valley}\right)>1$). However, it should be noted that while developing the phase map, the diffusivity, conductivity and transference number of PEO have been assumed in all cases. Realistically, electrolytes with different shear modulus

values show significant variation in transport properties, which can appreciably alter the form of this phase map.

To verify the validity of this phase map shown in Figure 6, some qualitative comparison with experimental results has been conducted. Some rough values of the elastic shear stiffness of PEO and poly-(styrene-ethylene-oxide) (SEO) polymer-based electrolytes have been estimated from their low-frequency storage modulus[20, 59]. The viscoelastic effect of polymer has not been taken into consideration due to the relatively slow deposition of lithium. The rate of operation and propensity of dendrite growth in PEO and SEO-based electrolytes have been adopted from Stone *et al.[20]* For electrolyte layer thickness ranging from 150μm to 300μm, the limiting current varied between 0.36mA/cm^2 and 0.72mA/cm$^{2[20]}$. For this range of limiting current and an applied current of 0.17mA/cm$^{2[20]}$, the range of operation, in terms of the ratio of applied current over limiting current $\left(i_{\text{applied}}/i_{\text{limiting}}\right)$ varies between 0.2 – 0.5. The range of elastic modulus values measured for PEO and SEO have been demonstrated in Figure 6 [20, 59]. As shown in the figure, during operation at applied current densities till 55% of the limiting value $\left(i_{applied} < 0.55 \times i_{\text{limiting}}\right)$, it is possible to have dendrite growth in PEO-based electrolytes, while SEO-based electrolytes should not allow growth of dendritic protrusions. Stone *et al.* observed similar results, where high modulus SEO polymer-based electrolytes cycled for long times, whereas PEO-based electrolytes experienced electrical short circuits very quickly[20]. It should be noted that, during comparison with the experimental data, the applied current has

been extracted as a fraction of the limiting current (similar to Figure 4). Also, the limited electrolyte domain considered in the simulation renders direct comparison of current density with experiments extremely difficult.

Ceramic based single ion conductors have been considered extensively as electrolyte in lithium ion batteries. Due to its extremely high elastic modulus, almost 100 times larger than that of lithium [63], it is assumed that ceramic-based single ion conductors will be able to prevent dendrite growth. However, due to the polycrystalline nature of the ceramics, they demonstrate grain/grain-boundary microstructure. The difference in mechanical and transport properties within the grain-interior and the grain-boundary region introduces heterogeneity within the ceramic electrolyte. It should be noted that the yield strength of ceramics are much higher than that of PEO based polymers. Also, the inherent anisotropy of ceramics at the grain level introduces additional complexity. The results demonstrated in Figure 6 assume that the yield strength of the material is independent of the elastic modulus. Hence, the present computational scheme developed for studying the homogeneous polymer electrolytes, cannot be used for modeling the ceramics simply by increasing the elastic modulus of the electrolyte domain. To accurately predict the propensity of dendrite growth within ceramic-based single ion conductor electrolytes, different simulations should be conducted with appropriate grain/grain-boundary microstructures and corresponding parameters that belong to ceramic materials.

Mechanism behind dendrite prevention: During operation at low current densities, suppression of dendrite growth with increasing shear modulus of the electrolyte phase can be attributed to the increase in compressive stress around the dendritic protrusion[21, 23]. However, even at higher current densities, the ratio of concentration/overpotential factors between protrusion peak and valley decreases significantly with rising electrolyte shear modulus (see the

red squares in Figure 5). This is possible only if the interfacial boundary between the lithium metal and polymer electrolyte changes significantly under high $G^{Electrolyte}$. The height of the dendritic protrusion (H) impacts the ratio of concentration/overpotential factors at the peak and the valley to a large extent. Variation in dendritic protrusion height with increasing shear modulus of the electrolyte phase has been plotted in Figure 7. The corresponding ratio between reaction current at the peak over that at the valley is shown by the red curve. For extremely low shear modulus values $\left(G^{Electrolyte} < 10^{-4} G^{Lithium}\right)$, no suppression of the dendritic protrusion is observed and its height remains unchanged at 800nm (the initial value). With increasing magnitude of electrolyte shear modulus $\left(10^{-4} G^{Lithium} < G^{Electrolyte} < 10^{-1} G^{Lithium}\right)$, the protrusion height drops sharply. In the third zone, where the electrolyte modulus is comparable to that of lithium $\left(G^{Electrolyte} > 10^{-1} G^{Lithium}\right)$, the protrusion height continues to decrease slowly. The corresponding vertical displacement contours within the lithium metal have also been shown in Figure 7 for three different values of the modulus. Here, the downward movement of the mesh

has been characterized as positive displacement. It is evident that the maximum displacement in the downward direction is observed at the protrusion peak. However, some upward displacement is also observed at the valley region during plastic flow of lithium. Due to symmetry boundary condition, displacement of metallic lithium in the horizontal direction at the left and right boundary has been prevented. Only vertical displacement is allowed there. During plastic deformation, lithium metal behaves as an incompressible material[57]. To conserve volume, downward deformation of the protrusion peak is matched with upward displacement of the protrusion valley. In other words, lithium metal flows under externally applied load from the protrusion peak to the valley region. Eventually, the plastic flow of lithium leads to suppression of the dendritic protrusion.

The existence of three different regions in Figure 7 can be explained based on the fact that the yield strengths of PEO-based polymers $\left(\sigma_{0,PEO} \sim 0.75MPa\right)$ are almost twice that of lithium metal $\left(\sigma_{0,Li} \sim 0.4MPa\right)$. In the first region, where the electrolyte shear modulus is significantly smaller than that of lithium $\left(G^{Electrolyte} < 10^{-4} G^{Lithium}\right)$, the effective stresses that evolve within the lithium and electrolyte always remain below the corresponding yield limits (see Figure S5(a)). Hence, only elastic deformation occurs within the lithium metal and polymer, which leads to insignificant change in the protrusion height. In the second regime, which exhibits

a rapid decrease in protrusion height, the shear modulus of polymer electrolyte is approximately two to three orders of magnitude smaller than that of lithium $\left(10^{-4}G^{Lithium} < G^{Electrolyte} < 10^{-1}G^{Lithium}\right)$. Here, the effective stress that evolves within lithium metal exceeds its yield limit and plastic deformation is observed (see Figure S5(b)). However, the effective stress within the polymer electrolyte remains below its yield strength, which gives rise to only elastic stresses. Hence, rapid flow of lithium metal due to plastic deformation and negligible flow of the polymer electrolyte phase leads to the drastic decrease in protrusion height. Finally, for electrolyte shear modulus values comparable to that of lithium metal $\left(G^{Electrolyte} > 10^{-1}G^{Lithium}\right)$, the magnitudes of effective stress that evolve in the lithium and polymer electrolyte exceed their yield strengths (demonstrated in Figure S5(c)). Hence, plastic flow occurs in lithium metal as well as PEO-based polymer. As a result, the reduction in protrusion height continues with increasing electrolyte modulus, but at a smaller rate than before. Due to the plastic deformation of polymer, the electrolyte material flows when initially pushed into contact with the lithium. This additional plastic flow of the electrolyte region reduces the need for additional deformation and flow of the lithium. This results in suppression of the lithium dendritic protrusion at a lower rate. It is evident from the displacement contour plots (shown in Figure 7) that the bottom of the lithium metal experiences negligible deformation, which is consistent with the zero-displacement boundary condition, applied there.

Comparing the black and the red curves in Figure 7, it is evident that effective suppression of the dendritic protrusion occurs in the second regime where elastic deformation of the polymer electrolyte is accompanied with plastic flow of the lithium protrusion (also see Figure S5). In this domain, significant decrease of the protrusion height has been observed even with minor increase in the electrolyte shear modulus. Rapid reduction in the protrusion height triggers a significant drop in the ratio of concentration/overpotential factor of reaction current between the peak and the valley. Hence, the ratio of total current at the peak over that at the valley $\left(i_{peak}/i_{valley}\right)$ also decreases quickly during plastic flow of the dendritic protrusion.

According to the shear modulus of PEO $\left(G^{Electrolyte}=7.7\times10^{-3}\times G^{Lithium}\right)$, this polymer electrolyte belongs to the second regime. However, due to the yield strength of PEO considered in this study $\left(\sigma_{0,PEO}\sim0.75MPa\right)$, it is not possible to completely suppress the dendrite growth during elastic deformation of the polymer electrolyte. This is manifested by the fact that the ratio of current between peak and valley is greater than unity even at the end of the second regime (follow the red curve in Figure 7).

All else being equal, increasing the yield limit for the polymer should extend its capacity for elastic deformation, making suppression of dendrites possible at lower values of the electrolyte modulus. Figure 8 demonstrates that by increasing the yield strength of polymer

electrolytes by approximately three times $\left(\sigma_{0,Elec} \sim 2.25 MPa\right)$, it is possible to obtain dendrite-free deposition of lithium even with an electrolyte shear modulus approximately two orders of magnitude smaller than that of lithium $\left(G^{Electrolyte} > 3\times 10^{-2} G^{Lithium}\right)$. Due to the increase in yield strength of the electrolyte phase, complete prevention of dendrite growth is seen within the intermediate region $\left(10^{-4} G^{Lithium} < G^{Electrolyte} < 10^{-1} G^{Lithium}\right)$, where plastic deformation of lithium is accompanied by elastic deformation of the polymer. Rapid plastic flow of the lithium metal leads to suppression of the dendritic protrusion to such an extent that the overall current at the peak becomes smaller than that at the valley $\left(i_{peak} < i_{valley}\right)$. This suppression of dendrites occurs for applied current densities at up to 75% of the limiting current.

Such modification of the yield strength of PEO-based polymers can be accomplished by the usage of several additives[48, 64]. However, for successful implementation of these PEO-based polymer composites as lithium-ion battery electrolytes, they must possess sufficiently large magnitudes of conductivity, diffusivity and transference number.

Conclusion

A detailed computational model has been developed to predict the propensity of lithium dendrite growth by coupling mechanical equilibrium, charge balance and mass conservation equations[21, 23, 51, 52]. Current density at the lithium electrolyte interface has been estimated from a modified version of the nonlinear Butler-Volmer relation that takes into account the surface curvature and mechanical stress-induced effects[23, 42]. The majority of the simulations have been conducted assuming transport and mechanical properties of bulk lithium metal and PEO polymer-based electrolyte[12, 47-49]. A perfect interface between the lithium foil and polymer electrolyte has been assumed that does not contain any surface roughness or a solid-electrolyte-interphase (SEI) layer[35, 36]. Elastic-plastic deformation of both lithium and polymer has been observed for electrolytes with relatively high shear modulus values $\left(G^{Electrolyte} > 10^{-3} G^{Lithium}\right)$. Plastic flow of the dendritic protrusion encourages stable deposition of lithium[41, 45]. A phase map has also been developed that demarcates certain combination of design (shear modulus of electrolyte) and operational (applied current density) parameters, for which dendrite-free stable deposition of lithium is possible during the recharge process. Some of the major conclusions obtained from this specific study are provided below:

1. The magnitude of applied current density (as a fraction of the limiting current) determines the propensity of dendrite growth. For PEO polymer-based electrolytes, if the applied current is less than 40% of the limiting current $\left(i_{applied} < 0.4 i_{limiting}\right)$, dendrite growth should not occur.
2. Application of a mechanical stress field helps to prevent dendrite growth in two ways:

a. Higher compressive stress at the protrusion peak as compared to the valley leads to enhanced reaction current density at the protrusion valley.
b. For high shear modulus electrolytes $\left(G^{Electrolyte} > 10^{-3} G^{Lithium}\right)$, plastic deformation of the lithium metal reduces the height of the dendritic protrusion. This also decreases the concentration/overpotential factor of the reaction current density at the protrusion peak.

3. The yield strengths of the lithium metal and polymer electrolyte also affect dendrite growth. Increasing the yield strength of the electrolyte can stabilize the dendritic protrusions, even with a shear modulus two orders of magnitude smaller than that of lithium. Hence, measurement of only the elastic modulus of the polymer electrolyte may not be sufficient. We must also focus on the measurement of yield strengths of the electrolytes.

It is worth mentioning that a realistic three-dimensional dendritic protrusion would be cylindrical in shape, whereas the present two-dimensional simulations capture the behavior of a knife-edge-like model dendritic protrusion. It is expected that a three-dimensional needle-like structure would experience more localized external force than a two-dimensional object, which can significantly alter its state of hydrostatic and deviatoric stress. Similarly, the difference between two-dimensional and three-dimensional structures can significantly impact the potential and concentration profile around the dendritic protrusion, and subsequently the current distribution between the peak and the valley. However, the present two-dimensional analysis provides a good qualitative understanding of the interaction between different parameters (such as shear modulus and yield strength of polymer electrolytes) responsible for preventing the growth of dendritic protrusions.

Acknowledgements

The authors gratefully acknowledge support from the U. S. Department of Energy (DOE), Vehicle Technologies Office. Argonne National Laboratory is operated for DOE Office of Science by UChicago Argonne, LLC under contract number DE-AC02-06CH11357. Lawrence Berkeley National Laboratory is managed for DOE Office of Science by University of California under contract number DE-AC02-05CH11231.

References

1. Xu, W., et al., *Lithium metal anodes for rechargeable batteries*. Energy & Environmental Science, 2014. **7**(2): p. 513-537.
2. Cheng, X.B., et al., *A Review of Solid Electrolyte Interphases on Lithium Metal Anode*. Advanced Science, 2016. **3**(3).
3. Bai, P., et al., *Transition of lithium growth mechanisms in liquid electrolytes*. Energy & Environmental Science, 2016. **9**(10): p. 3221-3229.
4. Cheng, X.B. and Q. Zhang, *Dendrite-free lithium metal anodes: stable solid electrolyte interphases for high-efficiency batteries*. Journal of Materials Chemistry A, 2015. **3**(14): p. 7207-7209.
5. Shin, W.K., A.G. Kannan, and D.W. Kim, *Effective Suppression of Dendritic Lithium Growth Using an Ultrathin Coating of Nitrogen and Sulfur Codoped Graphene Nanosheets on Polymer Separator for Lithium Metal Batteries*. Acs Applied Materials & Interfaces, 2015. **7**(42): p. 23700-23707.
6. Takehara, Z., *Future prospects of the lithium metal anode*. Journal of Power Sources, 1997. **68**(1): p. 82-86.
7. Brissot, C., et al., *Dendritic growth mechanisms in lithium/polymer cells*. Journal of Power Sources, 1999. **81**: p. 925-929.
8. Harry, K.J., et al., *Influence of Electrolyte Modulus on the Local Current Density at a Dendrite Tip on a Lithium Metal Electrode*. Journal of the Electrochemical Society, 2016. **163**(10): p. A2216-A2224.
9. Li, W.Y., et al., *The synergetic effect of lithium polysulfide and lithium nitrate to prevent lithium dendrite growth*. Nature Communications, 2015. **6**.
10. Zheng, G.Y., et al., *Interconnected hollow carbon nanospheres for stable lithium metal anodes*. Nature Nanotechnology, 2014. **9**(8): p. 618-623.
11. Harry, K.J., D.Y. Parkinson, and N.P. Balsara, *Failure Analysis of Batteries Using Synchrotron-based Hard X-ray Microtomography*. Jove-Journal of Visualized Experiments, 2015(102).

12. Geng, H.Z., et al., *Fabrication and properties of composites of poly(ethylene oxide) and functionalized carbon nanotubes.* Advanced Materials, 2002. **14**(19): p. 1387-1390.
13. Orsini, F., et al., *In situ SEM study of the interfaces in plastic lithium cells.* Journal of Power Sources, 1999. **81**: p. 918-921.
14. Rosso, M., et al., *Onset of dendritic growth in lithium/polymer cells.* Journal of Power Sources, 2001. **97-8**: p. 804-806.
15. Aurbach, D., *Review of selected electrode-solution interactions which determine the performance of Li and Li ion batteries.* Journal of Power Sources, 2000. **89**(2): p. 206-218.
16. Tang, C.-Y. and S.J. Dillon, *In Situ Scanning Electron Microscopy Characterization of the Mechanism for Li Dendrite Growth.* Journal of the Electrochemical Society, 2016. **163**(8): p. A1660 - A1665.
17. Dolle, M., et al., *Live scanning electron microscope observations of dendritic growth in lithium/polymer cells.* Electrochemical and Solid State Letters, 2002. **5**(12): p. A286-A289.
18. Mehrotra, A., P.N. Ross, and V. Srinivasan, *Quantifying Polarization Losses in an Organic Liquid Electrolyte/Single Ion Conductor Interface.* Journal of the Electrochemical Society, 2014. **161**(10): p. A1681-A1690.
19. Hallinan, D.T., et al., *Lithium Metal Stability in Batteries with Block Copolymer Electrolytes.* Journal of the Electrochemical Society, 2013. **160**(3): p. A464-A470.
20. Stone, G.M., et al., *Resolution of the Modulus versus Adhesion Dilemma in Solid Polymer Electrolytes for Rechargeable Lithium Metal Batteries.* Journal of the Electrochemical Society, 2012. **159**(3): p. A222-A227.
21. Barai, P., K. Higa, and V. Srinivasan, *Effect of Initial State of Lithium on the Propensity for Dendrite Formation: A Theoretical Study.* Journal of the Electrochemical Society, 2017. **164**(2): p. A180 - A189.
22. Ferrese, A. and J. Newman, *Mechanical Deformation of a Lithium-Metal Anode Due to a Very Stiff Separator.* Journal of the Electrochemical Society, 2014. **161**(9): p. A1350-A1359.
23. Monroe, C. and J. Newman, *The impact of elastic deformation on deposition kinetics at lithium/polymer interfaces.* Journal of the Electrochemical Society, 2005. **152**(2): p. A396-A404.
24. Chang, H.J., et al., *Correlating Microstructural Lithium Metal Growth with Electrolyte Salt Depletion in Lithium Batteries Using Li-7 MRI.* Journal of the American Chemical Society, 2015. **137**(48): p. 15209-15216.
25. Cogswell, D.A., *Quantitative phase-field modeling of dendritic electrodeposition.* Physical Review E, 2015. **92**(1).
26. Love, C.T., O.A. Baturina, and K.E. Swider-Lyons, *Observation of Lithium Dendrites at Ambient Temperature and Below.* Ecs Electrochemistry Letters, 2015. **4**(2): p. A24-A27.
27. Rosso, M., et al., *Dendrite short-circuit and fuse effect on Li/polymer/Li cells.* Electrochimica Acta, 2006. **51**(25): p. 5334-5340.
28. Schauser, N.S., et al., *Lithium Dendrite Growth in Glassy and Rubbery Nanostructured Block Copolymer Electrolytes.* Journal of the Electrochemical Society, 2015. **162**(3): p. A398-A405.

29. Ely, D.R. and R.E. Garcia, *Heterogeneous Nucleation and Growth of Lithium Electrodeposits on Negative Electrodes*. Journal of the Electrochemical Society, 2013. **160**(4): p. A662-A668.
30. Zhang, S.S., *A review on the separators of liquid electrolyte Li-ion batteries*. Journal of Power Sources, 2007. **164**(1): p. 351-364.
31. Stark, J.K., Y. Ding, and P.A. Kohl, *Nucleation of Electrodeposited Lithium Metal: Dendritic Growth and the Effect of Co-Deposited Sodium*. Journal of the Electrochemical Society, 2013. **160**(9): p. D337-D342.
32. Barton, J.L. and J.O.M. Bockris, *The electrolytic growth of dendrites from ionic solutions*. Proceedings of the Royal Society of London. Series: A. , 1962. **268**: p. 485 - 505.
33. Diggle, J.W., A.R. Despic, and J.O.M. Bockris, *The Mechanism of the Dendritic Electrocrystallization of Zinc*. Journal of the Electrochemical Society, 1969. **116**(11): p. 1503 - 1514.
34. Chazalviel, J.N., *Electrochemical Aspects of the Generation of Ramified Metallic Electrodeposits*. Physical Review A, 1990. **42**(12): p. 7355-7367.
35. Monroe, C. and J. Newman, *Dendrite growth in lithium/polymer systems - A propagation model for liquid electrolytes under galvanostatic conditions*. Journal of the Electrochemical Society, 2003. **150**(10): p. A1377-A1384.
36. Akolkar, R., *Mathematical model of the dendritic growth during lithium electrodeposition*. Journal of Power Sources, 2013. **232**: p. 23-28.
37. Akolkar, R., *Modeling dendrite growth during lithium electrodeposition at sub-ambient temperature*. Journal of Power Sources, 2014. **246**: p. 84-89.
38. Chen, L., et al., *Modulation of dendritic patterns during electrodeposition: A nonlinear phase-field model*. Journal of Power Sources, 2015. **300**: p. 376-385.
39. Ely, D.R., A. Jana, and R.E. Garcia, *Phase field kinetics of lithium electrodeposits*. Journal of Power Sources, 2014. **272**: p. 581-594.
40. Liang, L.Y. and L.Q. Chen, *Nonlinear phase field model for electrodeposition in electrochemical systems*. Applied Physics Letters, 2014. **105**(26).
41. Lee, H., et al., *A simple composite protective layer coating that enhances the cycling stability of lithium metal batteries*. Journal of Power Sources, 2015. **284**: p. 103-108.
42. Monroe, C. and J. Newman, *The effect of interfacial deformation on electrodeposition kinetics*. Journal of the Electrochemical Society, 2004. **151**(6): p. A880-A886.
43. Chang, H.J., et al., *Investigating Li Microstructure Formation on Li Anodes for Lithium Batteries by in Situ Li-6/Li-7 NMR and SEM*. Journal of Physical Chemistry C, 2015. **119**(29): p. 16443-16451.
44. Gireaud, L., et al., *Lithium metal stripping/plating mechanisms studies: A metallurgical approach*. Electrochemistry Communications, 2006. **8**(10): p. 1639-1649.
45. Choudhury, S., et al., *A highly reversible room-temperature lithium metal battery based on crosslinked hairy nanoparticles*. Nature Communications, 2015. **6**.
46. Tu, Z.Y., et al., *Nanoporous Polymer-Ceramic Composite Electrolytes for Lithium Metal Batteries*. Advanced Energy Materials, 2014. **4**(2).
47. Schultz, R., *Lithium: Measurement of Young's Modulus and Yield Strength*. Fermilab-TM-2191, 2002: p. 1 - 6.

48. Moreno, M., et al., *Electrical and mechanical properties of poly(ethylene oxide)/intercalated clay polymer electrolyte*. Electrochimica Acta, 2011. **58**: p. 112-118.
49. Tariq, S., et al. *Li Material Testing - Fermilab Antiproton Source Lithium Collection Lens*. in *Proceedings of the 2003 Particle Accelerator Conference*. 2003. IEEE.
50. Dill, E.H., *Continuum MEchanics: Elasticity, Plasticity, Viscoelasticity*. 2006, Boca-Raton, FL: CRC Press, Taylor and Francis Group.
51. Newman, J. and K.E. Thomas-Alyea, *Electrochemical Systems*. 2004, Hoboken, NJ: John Wiley and Sons.
52. Rahn, C.D. and C.-Y. Wang, *Battery Systems Engineering*. 2013, West Sussex, UK: John Wiley and Sons.
53. Zeng, Z.Y., et al., *Visualization of Electrode-Electrolyte Interfaces in LiPF6/EC/DEC Electrolyte for Lithium Ion Batteries via in Situ TEM*. Nano Letters, 2014. **14**(4): p. 1745-1750.
54. Ghassemi, H., et al., *Real-time observation of lithium fibers growth inside a nanoscale lithium-ion battery*. Applied Physics Letters, 2011. **99**(12).
55. Sacci, R.L., et al., *Nanoscale Imaging of Fundamental Li Battery Chemistry: Solid-Electrolyte Interphase Formation and Preferential Growth of Lithium Metal Nanoclusters*. Nano Letters, 2015. **15**(3): p. 2011-2018.
56. Zhang, X.C., W. Shyy, and A.M. Sastry, *Numerical simulation of intercalation-induced stress in Li-ion battery electrode particles*. Journal of the Electrochemical Society, 2007. **154**(10): p. A910-A916.
57. Lemaitre, J. and J.L. Chaboche, *Mechanics of Solid Materials*. 1990: Cambridge University Press.
58. Deen, W.M., *Analysis of Transport Phenomena*. 1998, New York: Oxford University Press.
59. Mullin, S., et al., *High Elastic Modulus Polymer Electrolytes Suitable for Preventing Thermal Runaway in Lithium Batteries*, in *US 2009/0104523 A1*, U.S.P.A. Publication, Editor. 2009: USA.
60. Paunovic, M. and M. Schlesinger, *Fundamentals of Electrochemical Deposition*. Second ed. 2006, Hoboken, New Jersey: John Wiley and sons.
61. Gu, W.B. and C.Y. Wang, *Thermal-electrochemical coupled modeling of a lithium-ion cell*. Lithium Batteries, Proceedings, 2000. **99**(25): p. 748-762.
62. Lu, Y.Y., et al., *Ionic-Liquid-Nanoparticle Hybrid Electrolytes: Applications in Lithium Metal Batteries*. Angewandte Chemie-International Edition, 2014. **53**(2): p. 488-492.
63. Hsieh, C.L. and W.H. Tuan, *Elastic properties of ceramic-metal particulate composites*. Materials Science and Engineering a-Structural Materials Properties Microstructure and Processing, 2005. **393**(1-2): p. 133-139.
64. Thakur, A.K., *Mechanism for improvement in mechanical and thermal stability in dispersed phase polymer composites*. Ionics, 2011. **17**(2): p. 109-120.
65. LaFemina, N.H., et al., *The diffusion and conduction of lithium in poly(ethylene oxide)-based sulfonate ionomers*. Journal of Chemical Physics, 2016. **145**(11).
66. Mullin, S.A., et al., *Salt Diffusion Coefficients in Block Copolymer Electrolytes*. Journal of the Electrochemical Society, 2011. **158**(6): p. A619-A627.

67. Landesfeind, J., et al., *Direct Electrochemical Determination of Thermodynamic Factors in Aprotic Binary Electrolytes*. Journal of the Electrochemical Society, 2016. **163**(7): p. A1254-A1264.
68. Wu, S.L., et al., *Discharge Characteristics of Lithium Battery Electrodes with a Semiconducting Polymer Studied by Continuum Modeling and Experiment*. Journal of the Electrochemical Society, 2014. **161**(12): p. A1836-A1843.

List of Tables

Table: I. A list of the mechanical and transport parameters used in the present simulation is provided below along with the references from where they have been adopted.

List of Figures

Figure: 1. Schematic diagram of the computational domains used for solving the mechanics, concentration and potential problems. (a) Lithium and electrolyte meshes used to determine the stress evolution around the dendritic protrusion. Height of the dendritic protrusion is defined as the distance between the peak and the valley of the lithium metal. (b) Computational domain on which concentration and potential distributions were calculated. Influx of lithium ions was imposed at the top of the electrolyte. The bottom boundary of the lithium region served as a current collector. Reaction current density was determined by the Butler-Volmer equation at the lithium-electrolyte interface. Symmetric boundary conditions were used at the left and the right side for both lithium and electrolyte.

Figure: 2. (a) Comparison between experimentally measured and computationally predicted elastic–plastic response of bulk lithium metal. (b) Comparison between experimental and computational elastic–plastic stress–strain curve for bulk PEO. Molecular weight of PEO measured in the experiment is 30,000g/mol. A nonlinear strain hardening law has been adopted for both bulk lithium and polymer materials. The value of elastic modulus (E) has been adopted from other literature[12, 47, 49]. The values of yield strength, hardening modulus and hardening exponent have been obtained through fits to the experimental data.

Figure: 3. (a) Contour plot of the potential observed within the electrolyte at steady state. The applied current is 75% of the magnitude of limiting current. Since the conductivity of lithium metal is very high, the potential throughout the lithium metal is extremely close to zero. Hence, the potential in this region has not been shown. (b) Concentration of lithium ions within the electrolyte at steady state. The current applied is 75% of the limiting current. The initial concentration of lithium within the electrolyte has been assumed to be 300mol/m^3. The transport properties of lithium ions within PEO polymers have been assumed for the electrolyte phase.

Figure: 4. The ratio of current at the peak over that at the valley with respect to the applied current has been plotted for lithium deposition with PEO polymer-based electrolytes. Increasing

the applied current encourages dendrite growth. The blue horizontal line indicates the barrier below which stable deposition of lithium occurs and above which dendrites can grow. For PEO-based electrolytes, if the applied current is greater than 42% of the limiting current, present simulations predict that dendrites can grow. From the experimental data, ratio between applied current over limiting current can be obtained (the data points along the x-axis). Even though the exact ratio of current at the peak over that at the valley is not known, the fact whether dendrite growth occurs or not, can be extracted from the experimental results. The critical current density predicted in the present research qualitative correlates with the experimental observations.

Figure: 5. Ratio of current at the peak over that at the valley has been plotted with respect to the shear modulus of the electrolyte phase (black circles). The yield strength and other plasticity parameters of the electrolyte have been kept identical to that observed in PEO. The applied current is 75% of the limiting current for that particular system. The results indicate that suppression of dendrite growth is only possible by very high modulus electrolytes, with $G^{Electrolyte}$ approximately 20 times greater than that of $G^{Lithium}$. Comparison between the concentration/overpotential factor ratio (red-square line) and ratio between interfacial-stress factors (blue-triangle line) at the peak and valley of the dendritic protrusion has also been demonstrated here.

Figure: 6. A phase map of the applied current with respect to the shear modulus of the polymer electrolyte phase. This map indicates that by increasing the elastic modulus of the electrolyte it may be possible to operate the battery at higher currents without the formation of dendrites. Elastic properties of poly(ethylene oxide) (PEO) and poly(styrene ethylene oxide) (SEO) has been adopted form Mullin *et al.* [59].

Figure: 7. Demonstration of the decrease in protrusion height under elastic-plastic deformation of lithium metal (denoted by the black squares). The red circles indicate the corresponding ratio of reaction current at the protrusion peak over that at the valley. For very low electrolyte shear modulus values, only elastic deformation of both lithium and PEO is observed. As the elastic modulus of the polymer-based electrolyte phase increases, the stress within both lithium metal and electrolyte increase. Since the yield strength of lithium is smaller in magnitude than that of the PEO-based electrolyte, plastic deformation of lithium occurs first. For very high electrolyte shear modulus values, both lithium and the electrolyte material deform plastically. Displacement contour plots for three different points have been depicted in the figure. Downward displacement has been denoted as positive. Significant reduction in protrusion height occurs during the plastic deformation of lithium metal. Due to plastic incompressibility of lithium metal, some upward displacement is also observed near the valley region during plastic deformation.

Figure: 8. Ratio of current at the peak over that at the valley plotted with respect to the shear modulus of the electrolyte phase. Increasing yield strength of the electrolyte phase helps to stabilize the deposition of lithium. The applied current is 75% of the limiting current for that particular system. The overall curve can be divided into three different zones: a) Low electrolyte modulus, where only elastic deformation of lithium and electrolyte occurs. b) Medium electrolyte modulus, where elastic deformation of the electrolyte is accompanied with plastic deformation of lithium metal. c) High shear modulus of the electrolyte, where elastic-plastic deformation of both lithium and electrolyte occurs.

Table: I. A list of the mechanical and transport parameters used in the present simulation is provided below along with the references from where they have been adopted.

Name	Symbol	Unit	Value	Ref.
Surface energy	γ	J/m^2	1.716	[23, 35]
Lithium Young's modulus	E_{Li}	GPa	9.0	[23]
Lithium shear modulus	G^{Li}	GPa	3.4	[23]
Lithium Poisson's ratio	ν^{Li}	--	0.42	[23]
Yield strength of lithium	$\sigma_{0,Li}$	MPa	0.4	[47, 49]
Hardening modulus of lithium	H_{Li}	MPa	1.9	[47, 49]
Hardening exponent of lithium	m_{Li}	--	0.4	[47, 49]
PEO polymer Young's modulus	E_{PEO}	MPa	70.0	[12]
PEO polymer shear modulus	G^{PEO}	MPa	26.2	[12]
Electrolyte Poisson's ratio	ν^{Elec}	--	0.3	[23]
Yield strength of PEO polymer	$\sigma_{0,PEO}$	MPa	0.77	[12, 48]
Hardening modulus of PEO polymer	H_{PEO}	MPa	3.5	[12]
Hardening exponent of lithium	m_{PEO}	--	0.4	[12]
Partial molar volume of lithium	$\bar{V}_{Li}$	m^3/mol	$1.3\text{x}10^{-5}$	[23]
Partial molar volume of electrolyte salt	$\bar{V}_{Elec}$	m^3/mol	$1.674\text{x}10^{-4}$	[23]
Lithium diffusion coefficient	D_e	m^2/s	$1\text{x}10^{-12}$	[65, 66]
Lithium transference number	t_{Li^+}	--	0.3	[23, 35]
Thermodynamic factor	$\partial \ln f_{\pm}/\partial \ln c_e$	--	$1.0\text{x}10^{-3}$	[67]
Conductivity in PEO polymer	κ_{PEO}	S/m	See Eq. (S4)	[68]
Conductivity in lithium	σ_{Li}	S/m	$1.1\text{x}10^{7}$	[38]

Frequency	ω	m^{-1}	10^6	[31, 55]
Amplitude	A	nm	400.0	[31, 55]
Anodic and cathodic reaction rate constants	k_a, k_c	$\left(mol/m \times s^2\right)^{1/2}$	9.832×10^{-6}	[23, 35]
Anodic and cathodic transfer coefficients	α_a, α_c	--	0.5	[23, 35]
Domain length	L_x	m	$2\pi/\omega$	[23]
Universal gas constant	R	$J/mol-K$	8.314	--
Temperature	T	K	298.15	--

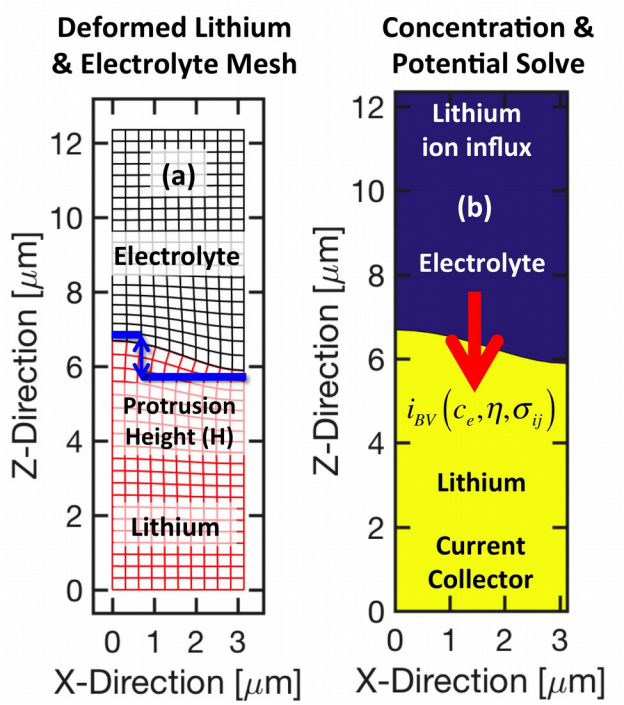

Figure: 1. Schematic diagram of the computational domains used for solving the mechanics, concentration and potential problems. (a) Lithium and electrolyte meshes used to determine the stress evolution around the dendritic protrusion. Height of the dendritic protrusion is defined as the distance between the peak and the valley of the lithium metal. (b) Computational domain on

which concentration and potential distributions were calculated. Influx of lithium ions was imposed at the top of the electrolyte. The bottom boundary of the lithium region served as a current collector. Reaction current density was determined by the Butler-Volmer equation at the lithium-electrolyte interface. Symmetric boundary conditions were used at the left and the right side for both lithium and electrolyte.

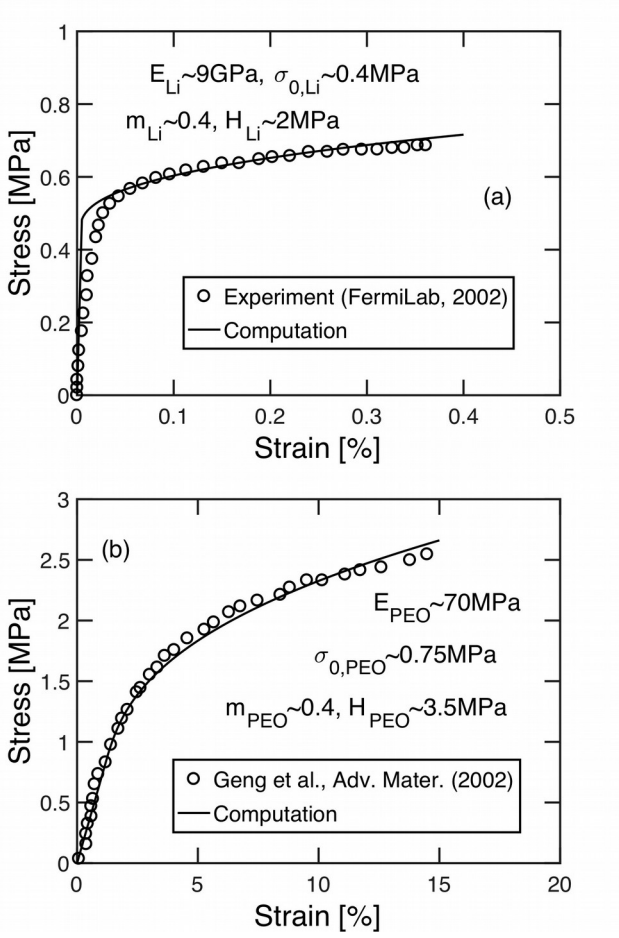

Figure: 2. (a) Comparison between experimentally measured and computationally predicted elastic–plastic response of bulk lithium metal. (b) Comparison between experimental and computational elastic–plastic stress–strain curve for bulk PEO. Molecular weight of PEO measured in the experiment is 30,000g/mol. A nonlinear strain hardening law has been adopted for both bulk lithium and polymer materials. The value of elastic modulus (E) has been adopted from other literature[12, 47, 49]. The values of yield strength, hardening modulus and hardening exponent have been obtained through fits to the experimental data.

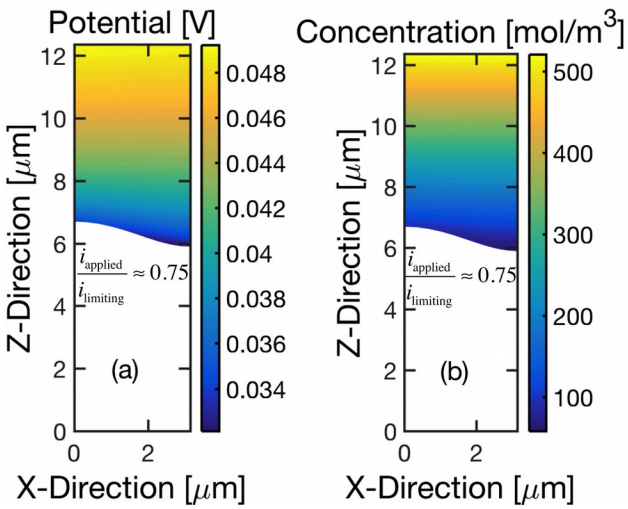

Figure: 3. (a) Contour plot of the potential observed within the electrolyte at steady state. The applied current is 75% of the magnitude of limiting current. Since the conductivity of lithium metal is very high, the potential throughout the lithium metal is extremely close to zero. Hence, the potential in this region has not been shown. (b) Concentration of lithium ions within the electrolyte at steady state. The current applied is 75% of the limiting current. The initial concentration of lithium within the electrolyte has been assumed to be 300mol/m^3. The transport properties of lithium ions within PEO polymers have been assumed for the electrolyte phase.

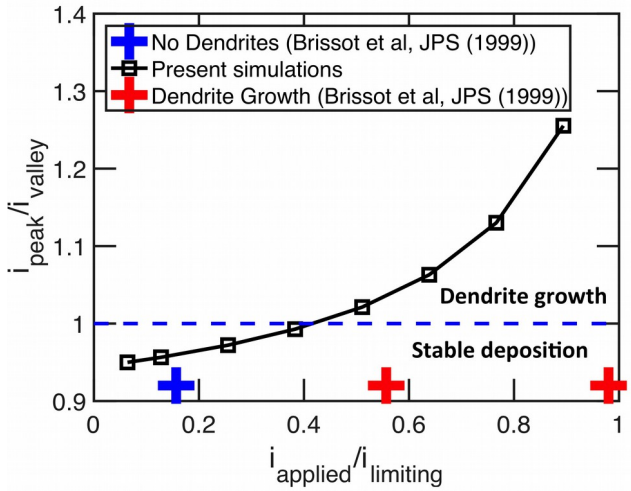

Figure: 4. The ratio of current at the peak over that at the valley with respect to the applied current has been plotted for lithium deposition with PEO polymer-based electrolytes. Increasing the applied current encourages dendrite growth. The blue horizontal line indicates the barrier below which stable deposition of lithium occurs and above which dendrites can grow. For PEO-based electrolytes, if the applied current is greater than 42% of the limiting current, present simulations predict that dendrites can grow. From the experimental data, ratio between applied current over limiting current can be obtained (the data points along the x-axis) [7]. Even though the exact ratio of current at the peak over that at the valley is not known, the fact whether dendrite growth occurs or not, can be extracted from the experimental results. The critical current

density predicted in the present research qualitative correlates with the experimental observations.

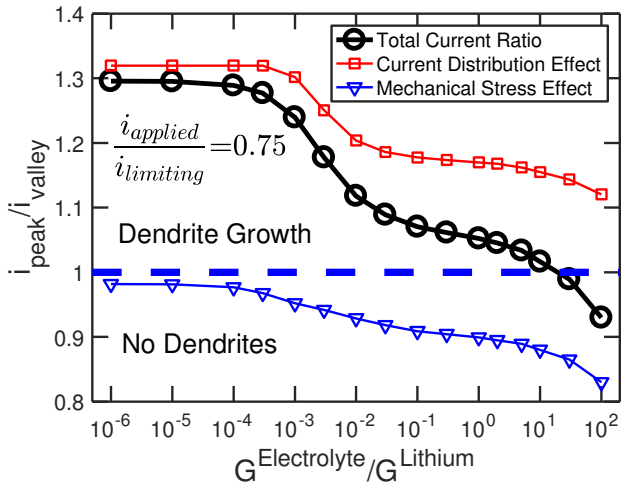

Figure: 5. Ratio of current at the peak over that at the valley has been plotted with respect to the shear modulus of the electrolyte phase (black circles). The yield strength and other plasticity parameters of the electrolyte have been kept identical to that observed in PEO. The applied current is 75% of the limiting current for that particular system. The results indicate that suppression of dendrite growth is only possible by very high modulus electrolytes, with $G^{Electrolyte}$ approximately 20 times greater than that of $G^{Lithium}$. Comparison between the concentration/overpotential factor ratio (red-square line) and ratio between interfacial-stress factors (blue-triangle line) at the peak and valley of the dendritic protrusion has also been demonstrated here.

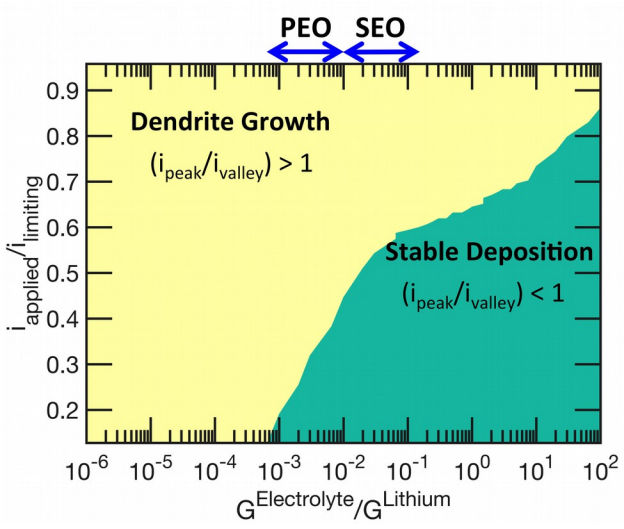

Figure: 6. A phase map of the applied current with respect to the shear modulus of the polymer electrolyte phase. This map indicates that by increasing the elastic modulus of the electrolyte it may be possible to operate the battery at higher currents without the formation of dendrites. Elastic properties of poly(ethylene oxide) (PEO) and poly(styrene ethylene oxide) (SEO) has been adopted form Mullin *et al.* [59].

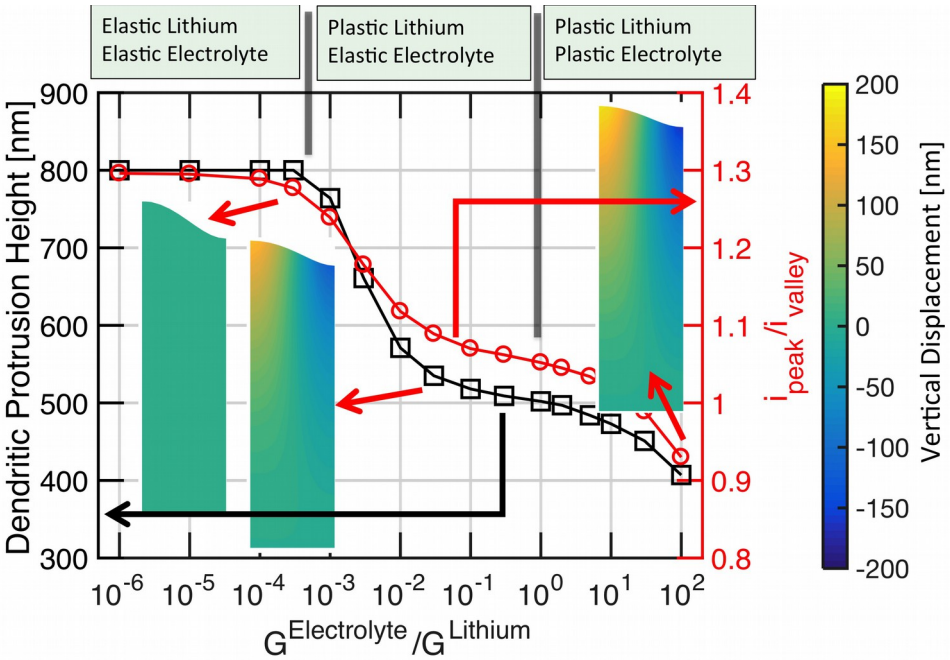

Figure: 7. Demonstration of the decrease in protrusion height under elastic-plastic deformation of lithium metal (denoted by the black squares). The red circles indicate the corresponding ratio of reaction current at the protrusion peak over that at the valley. For very low electrolyte shear modulus values, only elastic deformation of both lithium and PEO is observed. As the elastic modulus of the polymer-based electrolyte phase increases, the stress within both lithium metal and electrolyte increase. Since the yield strength of lithium is smaller in magnitude than that of

the PEO-based electrolyte, plastic deformation of lithium occurs first. For very high electrolyte shear modulus values, both lithium and the electrolyte material deform plastically. Displacement contour plots for three different points have been depicted in the figure. Downward displacement has been denoted as positive. Significant reduction in protrusion height occurs during the plastic deformation of lithium metal. Due to plastic incompressibility of lithium metal, some upward displacement is also observed near the valley region during plastic deformation.

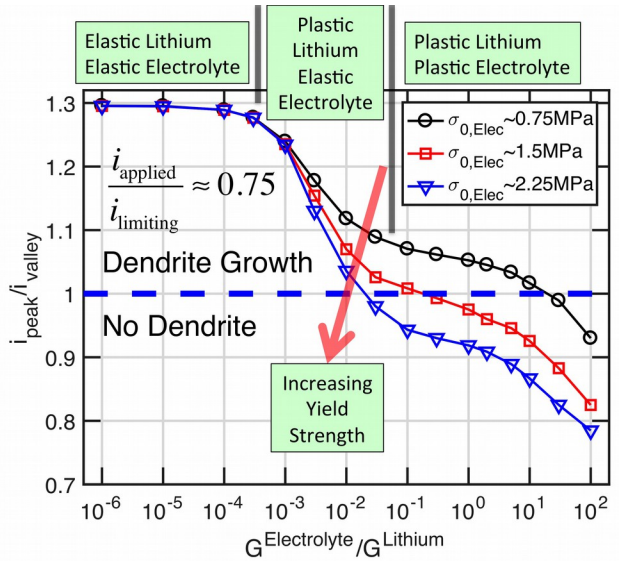

Figure: 8. Ratio of current at the peak over that at the valley plotted with respect to the shear modulus of the electrolyte phase. Increasing yield strength of the electrolyte phase helps to stabilize the deposition of lithium. The applied current is 75% of the limiting current for that particular system. The overall curve can be divided into three different zones: a) Low electrolyte

modulus, where only elastic deformation of lithium and electrolyte occurs. b) Medium electrolyte modulus, where elastic deformation of the electrolyte is accompanied with plastic deformation of lithium metal. c) High shear modulus of the electrolyte, where elastic-plastic deformation of both lithium and electrolyte occurs.